scientific reports

Check for updates

OPEN

Neuroprotective effect of NSCs-derived extracellular vesicles in Parkinson's disease models

Mercyleidi Díaz Reyes[1], Sabrina Gatti[1], Susana Delgado Ocaña[1], Hugo H. Ortega[2] & Claudia Banchio[1]✉

Parkinson's disease (PD) is a progressive neurodegenerative disorder characterized by both motor and non-motor symptoms, caused by the degeneration and loss of dopaminergic neurons in the *substantia nigra*. Current therapies are limited to symptom management, unable to prevent neuronal loss or halt the progression of the disease. A significant limitation to more effective treatments is the difficulty of crossing the blood-brain barrier (BBB). Extracellular vesicles (EVs) communication plays a crucial role in several physiological processes within the nervous system. Notably, EVs have the unique ability to cross the BBB, making them a highly promising vehicle for delivering therapeutic agents directly to the brain. Given the rising prevalence of PD, the need for therapies that prevent neuronal death and promote cell survival is urgent. This study explores the potential of neural stem cell-derived extracellular vesicles (NSC-EVs) using two in vitro models of PD. Our findings demonstrate that NSC-EVs significantly enhance the survival of dopaminergic neurons by reducing apoptosis and showing strong neuroprotective effects. Notably, the natural extracellular vesicles used in this study are enriched with Catalase, a potent scavenger protein with antioxidant properties. This natural enrichment further strengthens their neuroprotective capacity, enabling them to mitigate oxidative stress and protect vulnerable neurons. The use of such naturally enriched extracellular vesicles represents a promising approach for developing innovative therapies to effectively combat Parkinson's disease.

Parkinson's disease (PD) is the second most common neurodegenerative disorder that will affect approximately 13 million individuals worldwide in 2040[1]. It is characterized by rigidity, postural instability, resting tremors and non-motor symptoms like depression, anosmia, sleep disturbances and gastrointestinal changes[2]. Degeneration and loss of dopaminergic neurons in the *substantia nigra pars compacta* is the major cause of the symptoms. Neuronal death is the result of protein aggregation, chronic neuroinflammation with activated microglia cells, increased release of the pro-inflammatory cytokines, elevated concentration of reactive oxygen species (ROS) and mitochondrial dysfunction[3]. Currently, PD treatment is symptomatic and unable to prevent further loss of dopaminergic cells and reverse the pathology[4,5].

Extracellular vesicles (EVs) are nanosized bilayer lipid vesicles that are actively secreted by cells and can be derived from a wide range of cell sources. EVs carry as internal cargo many active biomolecules including nucleic acids, proteins, lipids and carbohydrates; and they also contain transmembrane-associated molecules[6]. The secretion of EVs was initially thought to be responsible for removing unwanted molecules from cells. However, recent studies showed that EVs are involved in a variety of intercellular signaling, mediating various physiological and pathological cellular processes by transporting different biomolecules and achieving intercellular exchange[7]. Considering that EVs can deliver bioactive molecules in long-distance intercellular communications and cross biological barriers, there is a growing interest in elucidating their role in the maintenance of homeostasis and regulation of cellular processes[8].

We have previously demonstrated that EVs derived from NSCs (NSC-EVs) enhance neuronal differentiation of NSCs and increase parameters associated with healthy neuronal function. In addition, we have evaluated the effect of these EVs under inflammation and oxidative stress, and the results indicate that, besides increasing neuronal differentiation, NSC-EVs treatment restores the morphology and function of the damaged neurons[9].

[1]Laboratorio de Biología Molecular y Celular de Lípidos, Instituto de Biología Molecular y Celular de Rosario (IBR-CONICET) Ocampo y Esmeralda, Predio CONICET and Departamento de Ciencias Biológicas, Facultad de Ciencias Bioquímicas y Farmacéuticas, Universidad Nacional de Rosario, 2000 Rosario, Argentina. [2]Centro de Medicina Comparada, ICiVet-Litoral, Universidad Nacional del Litoral-CONICET, 3080 Esperanza, Santa Fe, Argentina. ✉email: banchio@ibr-conicet.gov.ar

PD is the second cause of disability and morbidity, and the incidence of this disease will significantly increase in the following years, thus searching for effector molecules that prevent neuronal death or increase cell survival represents a key challenge in the treatment of this disease.

In this work, using two different in vitro models of PD, we demonstrate that NSC-derived EVs significantly increase the survival of dopaminergic neurons by decreasing ROS accumulation. The antioxidant effect observed is due to EVs delivery of the scavenger protein Catalase, suggesting that native NSC-derived EVs could be a tool for developing novel PD treatments.

Results

In vitro models of Parkinson's disease

To evaluate the effect of NSCs-derived EVs, we have established two PD models using the human cell line SH-SY5Y. The first model was established by selecting stable cell lines that overexpressed the wild-type protein (WT) or the mutant A53T Synuclein associated with the familiar disease type[10]. As a control, we used clones transfected with the empty vector (pcDNA3.1). Synuclein overexpression was confirmed by Western Blot (Supplementary Fig. 1a) and immunocytochemistry (Supplementary Fig. 1b). As was previously reported[11], A53T Synuclein overexpression changed the ratio of intracellular localization increasing the nuclear content of this variant (Supplementary Fig. 1c).

The second model was performed by the treatment with 6-hydroxydopamine (6-OHDA) which is specifically taken up by dopaminergic neurons through the dopamine transporter, and it is oxidized to produce free radicals, thus leading to neuronal death through mitochondrial dysfunction and oxidative stress[12]. We evaluated cell viability by MTT[13], and we observed a dose-dependent effect on cell survival (Supplementary Fig. 2). For the following studies, we selected 10 µM as the concentration that affects cell viability decreasing the survival to 41% compared with the control.

NSC-derived extracellular vesicles rescue cell viability of Synuclein-overexpressing cells

As neuronal death is the major cause of PD[3], we compared the viability of cells overexpressing Synuclein WT and the mutant A53T by MTT metabolic assay[13]. We found that overexpression of each of these proteins independently has an impact on cell survival and that the reduction in cell viability is more pronounced for cells overexpressing the A53T mutant version (Fig. 1a). Moreover, we directly quantified cell death by a double staining assay with the fluorescent probes Ethidium Bromide (EB) and Acridine Orange (AN)[14]. The quantification analysis showed that cells that overexpressed Synuclein proteins have a marked increase in apoptosis, being significantly higher for the A53T mutant (Fig. 1b).

Since PD is also associated with an increase in intracellular levels of ROS[3], we measured free oxygen radicals using the DCFH-DA probe followed by quantification of the fluorescence intensity signal (FI). We observed a significant increase of ROS levels in cells that overexpress both forms of Synuclein (Fig. 1c) suggesting that our in vitro PD model systems recapitulate key features present in the in vivo forms of the disease.

We have previously demonstrated that NSC-derived EVs promote NSC differentiation into neurons, and restore the aberrant morphology induced by inflammation[9]. To explore if NSC-EVs can rescue cell death of dopaminergic neurons in the PD models, we first evaluated if mouse-derived EVs are taken by the human neuroblastoma cell line SH-SY5Y. For this aim, we purified and characterized EVs derived from NSCs cultured under proliferation conditions as previously described[9] (see Material and Methods) (Fig. 2; Table 1), and labelled with FM 4–64 in a dilution (1:5). As a control we used the same volume of PBS containing the same dilution of the probe (1:5). We supplemented SH-SY5Y cells, and tracked the delivery of the probe by in vivo confocal

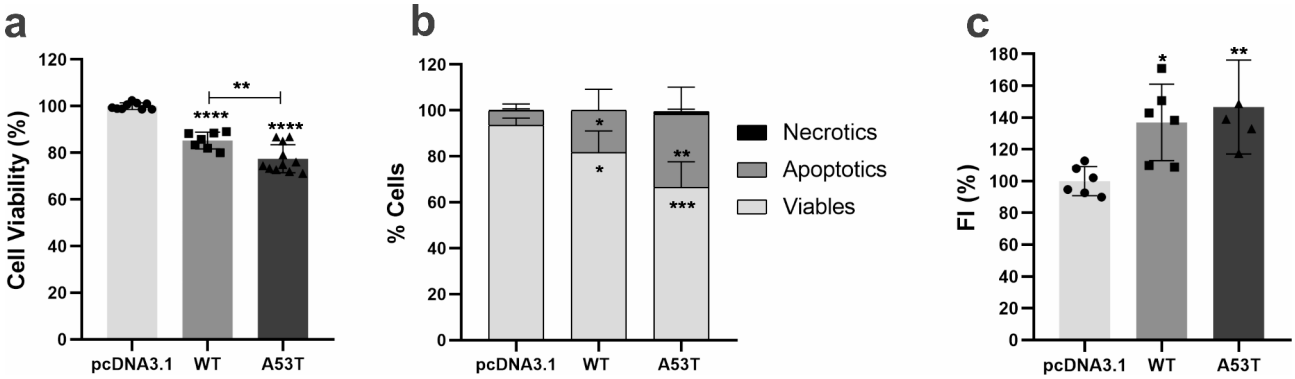

Fig. 1. Synuclein overexpression induces apoptosis and ROS accumulation. (**a**) Cells of the indicated clones (pcDNA3.1: SH-SY5Y pcDNA3.1; WT: SH-SY5Y pcDNA3.1-WT-α-Synuclein; A53T: SH-SY5Y pcDNA3.1-A53T-α-Synuclein) were incubated under differentiation for a period of 72 h, and cell viability was analyzed by MTT assay. Graph represents cell viability (%). (**b**) Percentage of viable, apoptotic and necrotic cells determined by double staining assay. (**c**) Effect of Synuclein overexpression on ROS levels measured by the florescence associate to the specific probe DCFH-DA, data is shown as percentage of fluorescence intensity (FI%). Results represent the mean ± S.D. of 3 independent experiments. One-Way ANOVA; Dunnett; * $p < 0.05$, ** $p < 0.01$, *** $p < 0.001$, **** $p < 0.0001$.

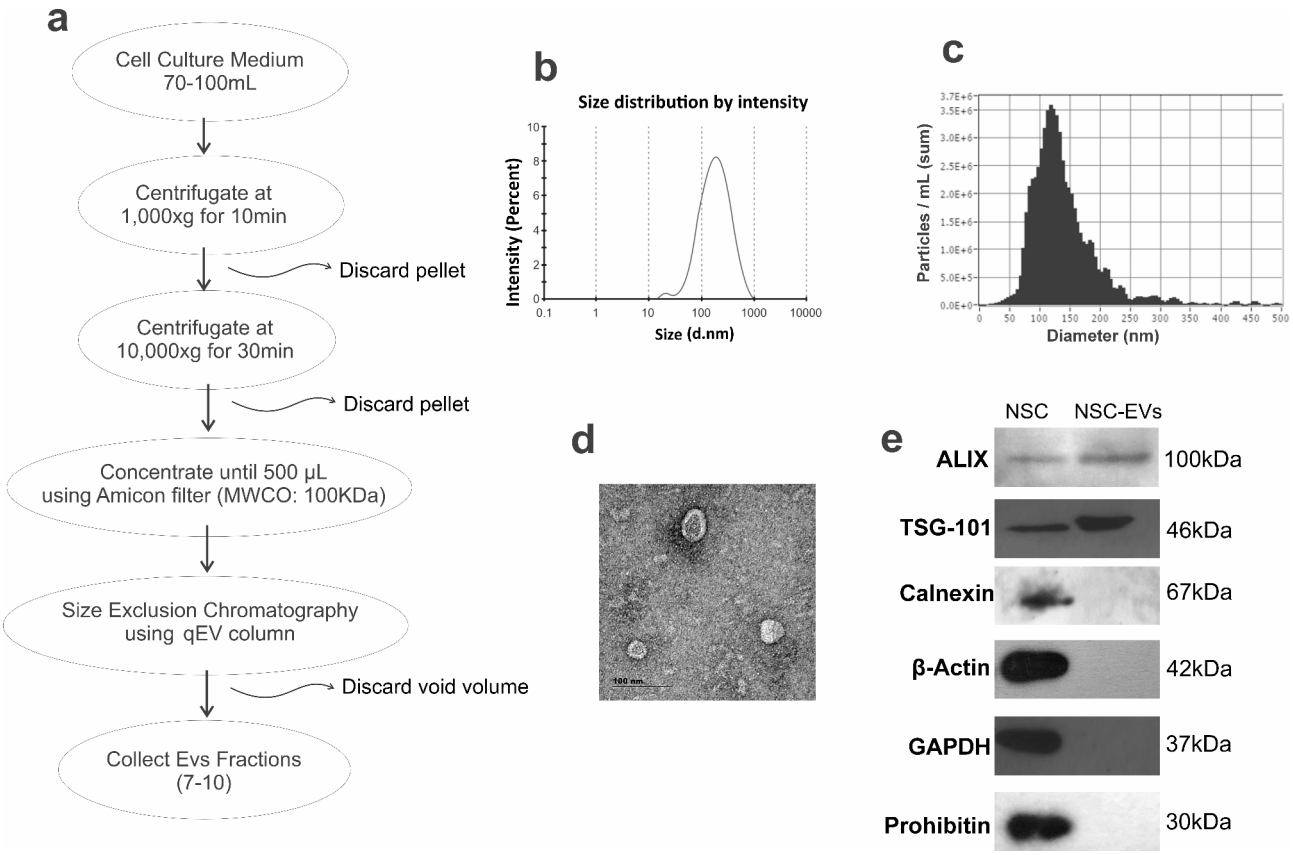

Fig. 2. NSC-EVs purification and characterization. (**a**) Schematic representation of EVs purification protocol. (**b**) Size distribution by Dynamic Light Scattering. (**c**) Concentration and size distribution by Nanoparticle Tracking Analyzer (NTA) (**d**) Representative image of the morphological analysis done by transmission electron microscopy (TEM) (**e**) Representative Western blot of exosome protein marker. The figure displayed here are cropped from the same gels/blot, and without high-contrast (overexposure).

Protein Name	Gen	Uniprot ID
Heat shock protein HSP 90-alpha	Hsp90aa1	P07901
Heat shock protein HSP 90-beta	Hsp90ab1	P11499
CD81 antigen	Cd81	P35762
CD9 antigen	Cd9	P40240
Tumor susceptibility gene 101 protein	Tsg101	Q61187
Multivesicular body subunit 12B	MVB12B	Q9H7P6
Vacuolar protein sorting-associated protein 37B	VPS37B	Q9H9H4
Charged multivesicular body protein 4b	Chmp4b	Q9D8B3
Programmed cell death 6-interacting protein	Pdcd6ip	Q9WU78

Table 1. Specific markers of small extracellular vesicles and proteins involved in their biogenesis and secretion identified by mass spectrometry analysis in NSC-EVs.

microscopy analysis[9]. As the Supplementary video and Fig. 3a and b show, cells become fluorescent only when they are treated with FM4-64-labelled NSCs-EVs. The measurement of the membrane-associated fluorescence shows a time-dependent increase with a peak at 100 s followed by a slow but significant decrease up to mostly the initial level. The results suggest that the increase in cytoplasmatic fluorescence confirms NSC-EVs delivery to the cells (Fig. 3c). In contrast, control cells labelled with PBS-FM4-64 incorporate very little of the probe represented by low fluorescence (Fig. 3b, d and e). Moreover, the fluorescence did not decrease, suggesting that the free probe is incorporated into the cellular membrane (Fig. 3d). In concordance, very little amount of fluorescence can be detected in the cytoplasm (Fig. 3e). This result confirmed that NSC-EVs target by neuronal SH-SY5Y cells.

We then evaluated if NSC-EVs treatment could affect the viability of neurons that overexpressed each Synuclein variant. Cells were grown for 24 h under proliferation conditions, and then the media was replaced

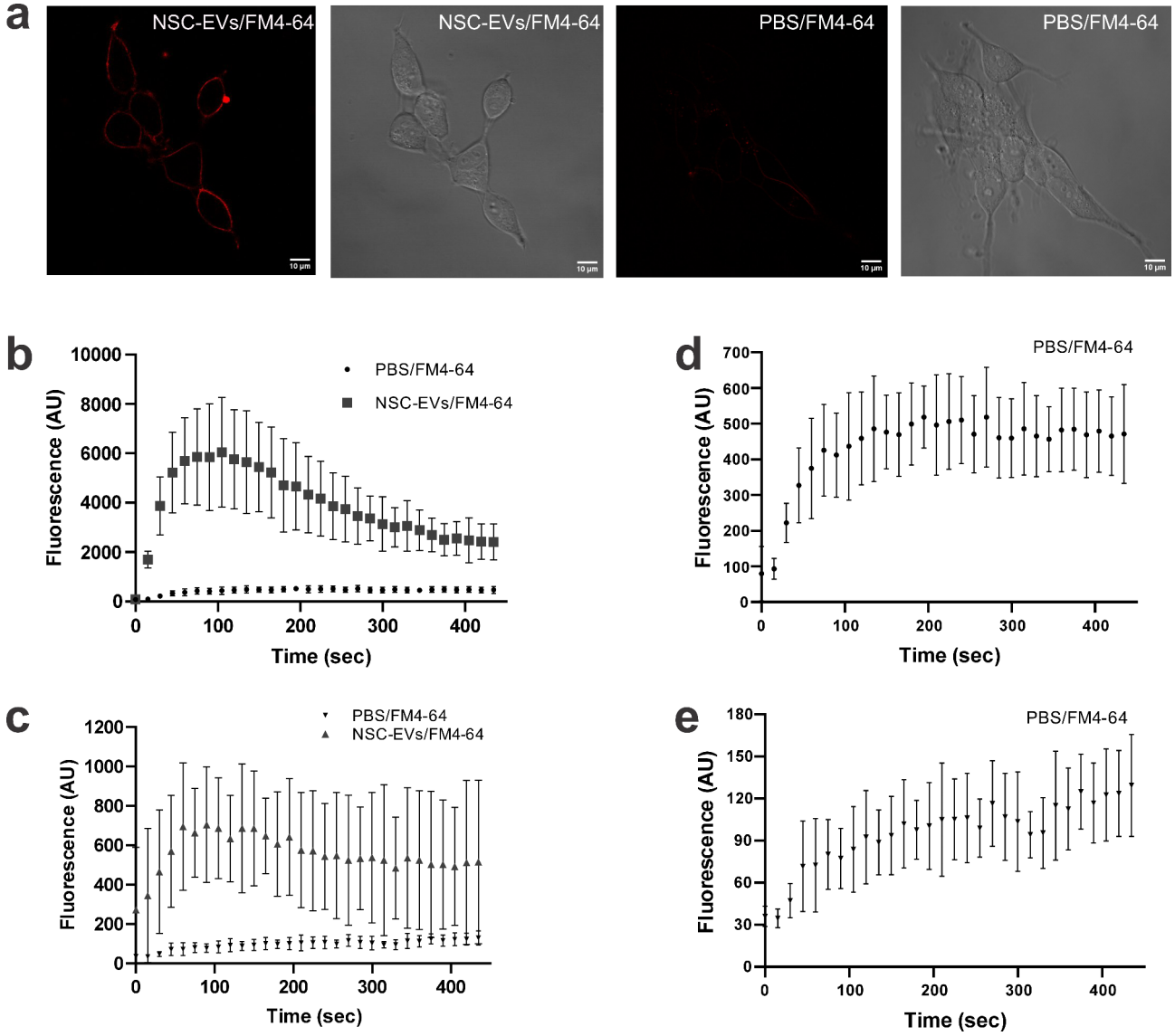

Fig. 3. SH-SY5Y cells internalize NSC-EVs. (**a**) Representative microphotographs of SH-SY5Y after addition of NSC-EVs labeled with FM® 4–64. Note that increased red fluorescence indicates internalization of EVs. (**b**) Membrane fluorescence intensity at different time point of cells treated with labelled EVs (NSC-EVs/FM4-64) or PBS supplemented with the probe (PBS/FM4-64). (**c**) Intracellular fluorescence intensity at different time points in cells treated with NSC-EVs/FM4-64 or PBS/FM4-64. (**d**) Membrane fluorescence intensity at different time point in cells treated with probe in PBS/FM4-64. (**e**) Intracellular fluorescence intensity at different time points in cells treated with PBS/FM4-64.

with differentiation media and incubated for 48 h. Differentiating cells were supplemented with or without NSC-EVs (3×10^5 particles/µL) for 48 h and at this time cell viability was determined by MTT assay[13]. We observed that NSC-EVs increased cell survival in wild-type and mutant Synuclein-expressing clones. Interestingly, the treatment restored the percentage of cell viability to control levels (Fig. 4). In addition, by double staining assay, we quantified the percentage of cells that died by necrosis or apoptosis and the percentage of viable cells in the presence or in absence of NSC-EVs. We demonstrated that NSC EVs-treated cells have an increased viability due to a decrease in apoptosis and specifically, for the A53T mutant, in necrosis (Fig. 5). Similar results were described using EVs derived from human umbilical cord mesenchymal stem cells[15].

One of the main characteristics of PD is ROS accumulation causing mitochondrial dysfunction and cell death[3]. As previously shown, Synuclein overexpression led to increased ROS levels determined using the fluorescence intensity of the specific probe DCFH-DA (Fig. 1c). Since NSC-EVs treatment restores cell viability to control levels (Fig. 4) and reduces apoptosis (Fig. 5b), we investigated whether these effects might be linked to changes in ROS levels in these cell lines. Interestingly, when measuring ROS levels after 48 h of NSC-EVs treatment, the levels of FI in cells overexpressing Synuclein decreased up to the control (Fig. 6), suggesting

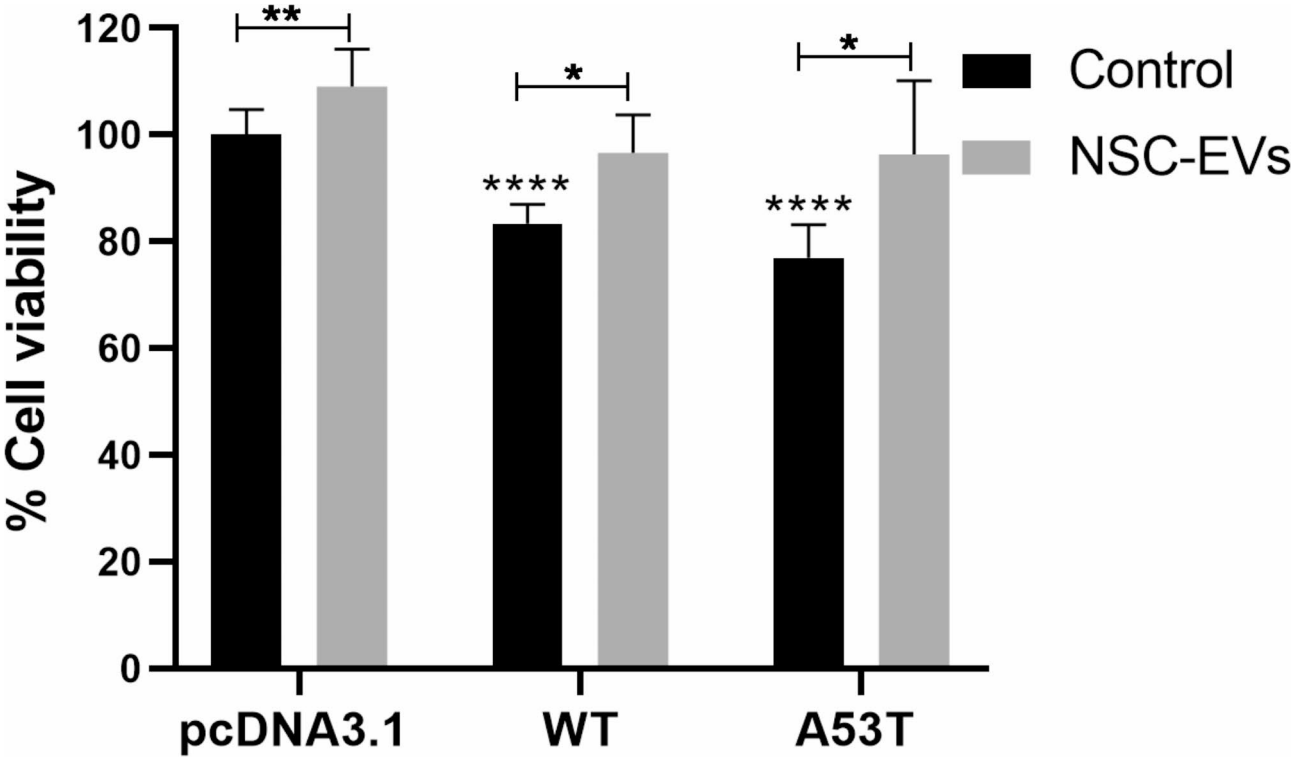

Fig. 4. NSC-EVs improve the survival of cells overexpressing α-Synuclein. MTT assay of each clone cultured during 72 h under differentiation conditions in the presence or in the absence of NSC-EVs. Graph represents the mean +/- SD of 3 experiments. One-Way ANOVA; Tukey; * $p < 0.05$, ** $p < 0.01$, **** $p < 0.0001$. pcDNA3.1: SH-SY5Y pcDNA3.1; WT: SH-SY5Y pcDNA3.1-WT-α-Synuclein; A53T: SH-SY5Y pcDNA3.1-A53T-α-Synuclein; NSC-EVs: extracellular vesicles derived from neural stem cell.

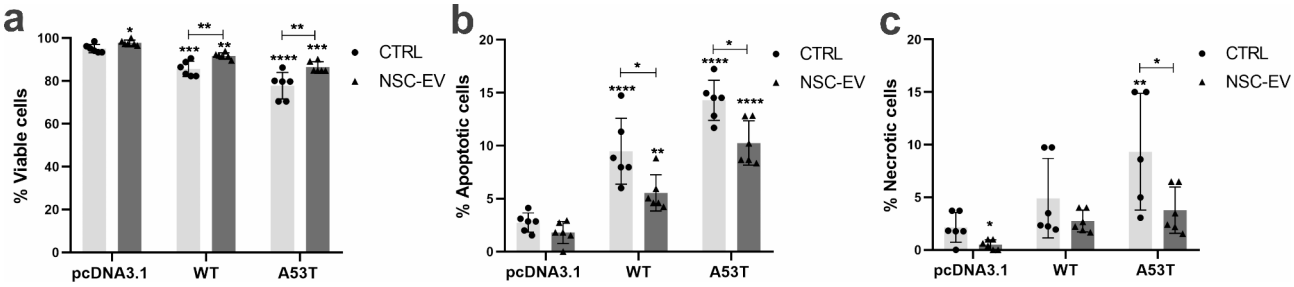

Fig. 5. Effect of NSC-EVs on cell death. Graph represents the percentage of viable (**a**), apoptotic (**b**) and necrotic (**c**) cells determined by double staining assay in cultures of alfa-Synuclein expressing clones incubated for 72 h under differentiation conditions in presence or in the absence of NSC-EVs. Results represent the mean +/- SD of 3 independent experiments of 10 images each. One-Way ANOVA; Tukey; * $p < 0.05$, ** $p < 0.01$, *** $p < 0.001$, **** $p < 0.0001$. pcDNA3.1: SH-SY5Y pcDNA3.1; WT: SH-SY5Y pcDNA3.1-WT-α-Synuclein; A53T: SH-SY5Y pcDNA3.1-A53T-α-Synuclein; NSC-EVs: extracellular vesicles derived from neural stem cell.

that NSC-EVs have an impact on ROS-associated cell damage which plays a deleterious effect in dopaminergic neurons in PD.

NSC-derived extracellular vesicle restores cell viability in the 6-OHDA Parkinson's disease model

The PD model established by treating the SH-SY5Y cells with 6-OHDA (10μM) showed that it significantly affects dopaminergic neurons survival (Supplementary Fig. 2). We also quantified cell death and demonstrated that cells treated with 6-OHDA can undergo either apoptosis or necrosis (Fig. 7a). Expression of Synuclein proteins assayed by immunocytochemistry (see Material and Methods), and quantification of fluorescence intensity with Image J (NIH), showed that 6-OHDA treatment increases Synuclein expression without affecting

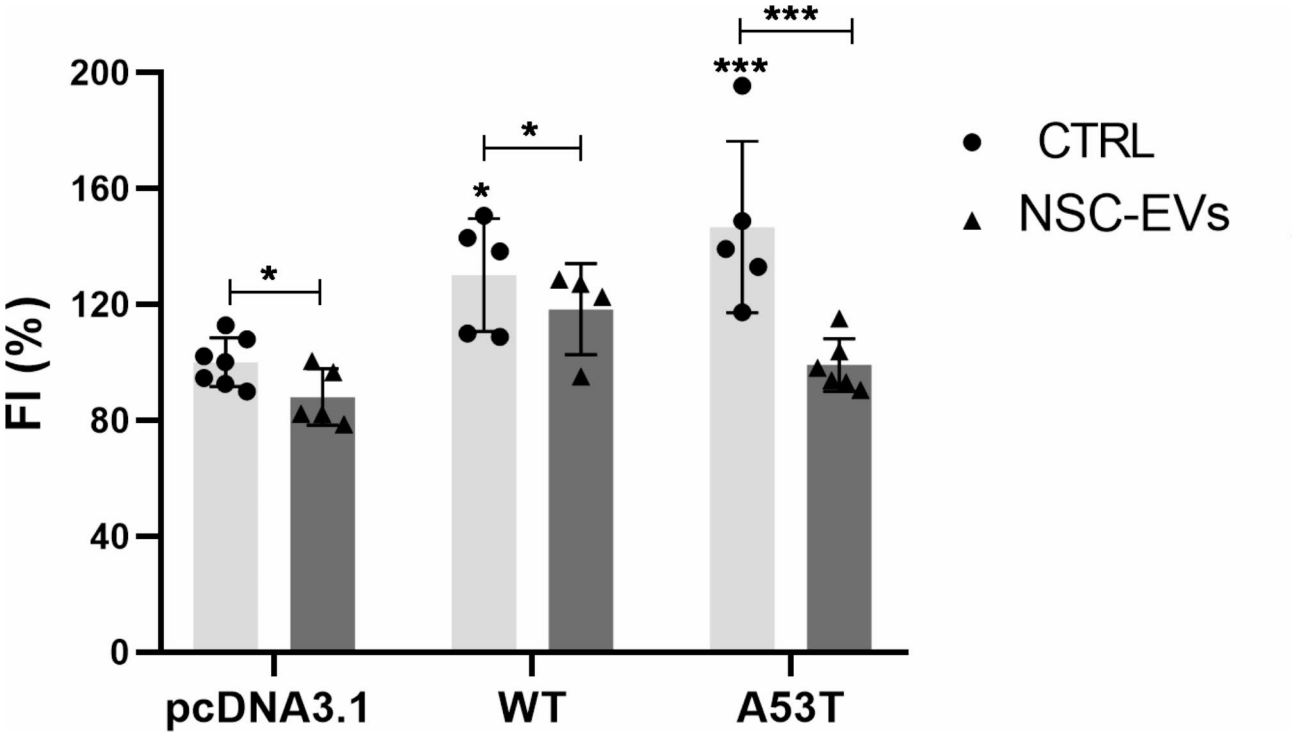

Fig. 6. NSC-EVs decreases ROS levels. Quantification of ROS through DCFH-DA fluorescence intensity (FI %) in cultures of the indicated clones (pcDNA3.1: SH-SY5Y pcDNA3.1; WT: SH-SY5Y pcDNA3.1-WT-α-Synuclein; A53T: SH-SY5Y pcDNA3.1-A53T-α- Synuclein) incubated for 72 h under differentiation conditions in the presence or in the absence of NSC-EVs. One-Way ANOVA; Tukey; * $p < 0,05$, *** $p < 0,001$.

its cellular localization (Fig. 7b and c). Then, we measured ROS levels as described above and observed an increase in free oxygen radicals, as expected from the mechanism of action of 6-OHDA (Fig. 8).

To evaluate if NSC-EVs can rescue cellular damage induced by 6-OHDA treatment, we incubated cells in the presence of NSC-EVs (3×10^5 particles/μL) for 32 h before 6-OHDA treatment. After 16 h, cell viability was assayed by MTT and compared with culture treated with PBS as a control. As Fig. 9a and b show, NSC-EVs pretreatment rescues 6-OHDA-induced cell death, restoring cell viability. Interestingly, NSC-EVs pretreatment also decreases ROS accumulation (Fig. 9c), suggesting that EVs can deliver biomolecules that protect cells from oxidative stress. To confirm this hypothesis, we evaluated if these EVs could revert the damage induced by this drug. To this aim, we incubated cells in the presence of 6-OHDA (10μM) for 8 h, after that, the media was changed and replaced with media supplemented with NSC-EVs (3×10^5 particles/μL). After 40 h, cell viability was assayed by MTT and compared with cultured cells treated with PBS (control). As Fig. 10 shows, NSC-EVs partially rescue cell viability and significantly decreased ROS accumulation (Fig. 10c).

NSCs-EVs carry Catalase

As the results demonstrated that NSC-EVs decrease ROS levels in dopaminergic neurons (Figs. 6, 8 and 9), a phenotype associated with PD[16]and ageing[17], we investigated if NSC-EVs carry antioxidant enzymes.

To identify the antioxidant proteins, we performed a proteomic analysis of NSC-EVs. For this, EVs-purified proteins were subjected to tryptic digestion as previously described[18]. The resulting peptides were then processed using a mass spectrometer coupled with a nano HPLC system for peptide separation and protein identification. As shown in Table 2, NSC-EVs are enriched in catalase and other proteins involved in oxidative defense. This finding underscores the potential of NSC-EVs to confer protective effects against oxidative damage.

As Catalase is the major enzyme involved in oxidative clearance[19], a successful brain delivery of catalase as PD therapy could represent an interesting avenue to be investigated. To confirm that EVs derived from NSCs deliver active catalase enzyme, we performed Western blot analysis and measuredCatalase activity. For Western blots, we loaded NSC-EVs (15 μg containing protein), total protein extract from NSCs (15 μg) and, as a control, pure Catalase (SIGMA) (0.1 μg) and we used an anti-Catalase antibody (Abcam) as describe in Material and Methods. As shown in Fig. 11a, NSC-EVs carry abundant levels of Catalase. In addition, the catalase-peroxidase activity assay through native PAGE was performed as described in the methods[20–22]. Briefly, the gel was incubated with hydrogen peroxide and stain gel with 2% potassium ferricyanide and 2% iron chloride. The peroxide is oxidized to molecular oxygen, the green color begins to appear on the gel, and the Catalase bands appear clear or yellow on the green background of the gel. The results shown in Fig. 11b indicate that the Catalase carried by NSC-EVs is in its active form.

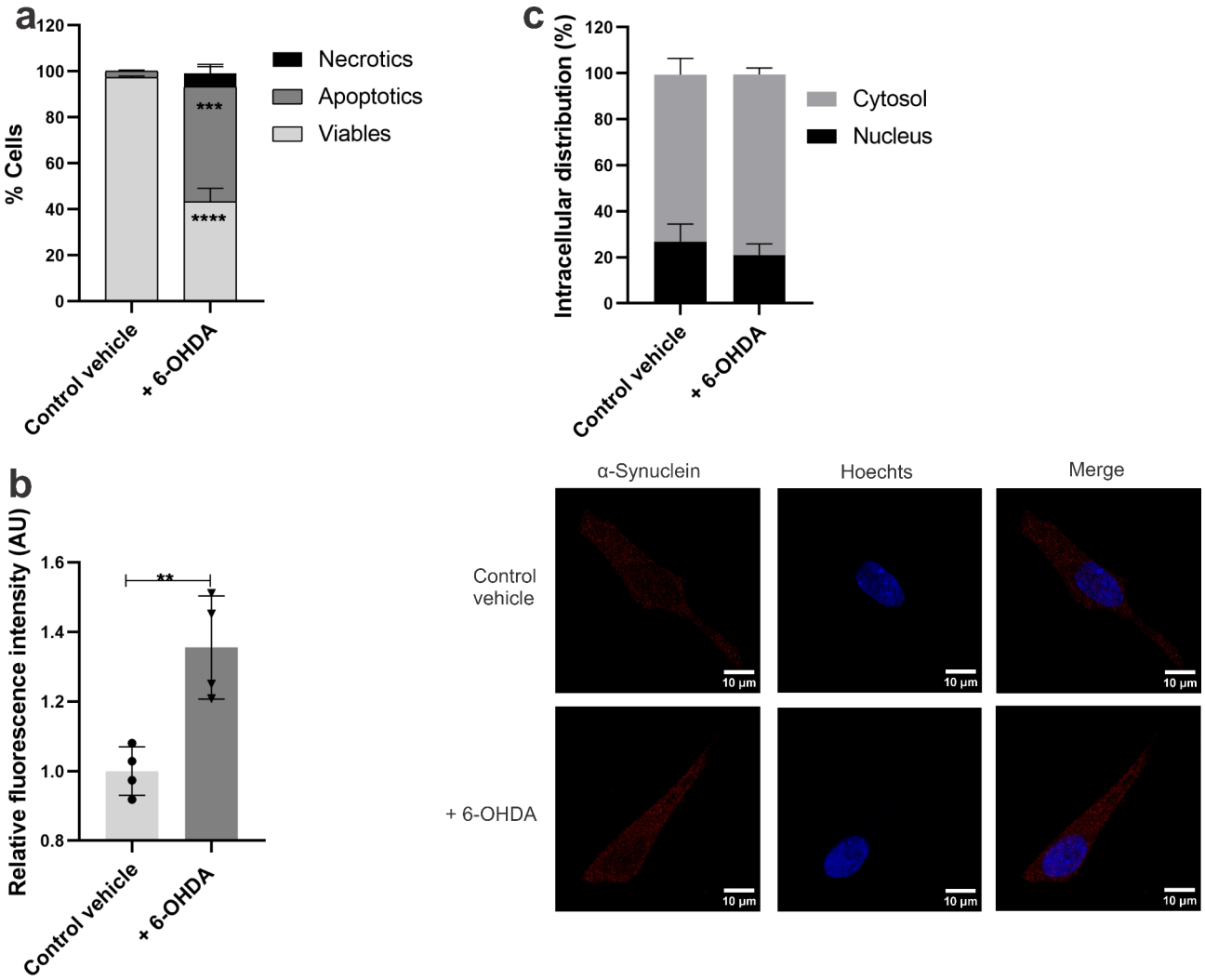

Fig. 7. Effect of 6-OHDA on cell death and ROS accumulation. (**a**) Percentage of viable, apoptotic and necrotic cells obtained by double staining assay of SH-SY5Y cell cultures incubated under differentiation conditions and treated with 10 µM of 6-OHDA. (**b**) Levels of alfa-Synuclein expression and (**c**) intracellular localization in SH-SY5Y cells treated with 6-OHDA. Representative images of each condition. Results represent the mean +/- SD of 3 experiments of 10 images (t-test; $^{**}p < 0.01$, $^{***}p < 0.001$ $^{****}p < 0.0001$). 6-OHDA: 6-hydroxydopamine.

Discussion

Cells usually communicate with one another through direct interactions or by releasing growth factors, trophic factors, and cytokines. Recently, EVs, like exosomes, have been acknowledged as powerful tools for intercellular communication, as they are secreted by almost all cell types and can be extracted from conditioned cell media or bodily fluids[23]. Although exosomes carry a common set of evolutionarily conserved proteins, such as tetraspanins, Alix, and Tsg101 (Table 1; Fig. 2), indicating they have similar biological activities, they also contain specific proteins. This suggests that they have distinct and unique biological functions depending on the cell source and the context in which these are released. Mesenchymal stem cells-derived EVs have anti-inflammatory, immune-regulatory, anti-apoptotic, and micro-vascular regeneration effects, with potential therapeutic effects against PD[24].

In our study, we have proved that mouse-derived NSCs-EVs are taken up by human SH-SY5Y cells showing that NSCs-EVs are captured by neurons even when these are derived from cross-species sources (Fig. 3). The demonstrated crosstalk between mouse and human cells reinforce that EVs are a novel mode of cross-species interaction[25]. Similar example include plant derived EVs and human cells[26,27], or bacteria derived EVs that promote skin inflammation[28] or lung injury[29].

We have previously demonstrated that NSCs-derived EVs promote NSCs proliferation and induce NSCs differentiation into functional neurons. EVs also restore parameters associated with neuronal function like Synaptophysin expression and dendritic spines density[9]. In addition, EVs restore cellular damage in NSCs under inflammation and oxidative stress increasing the survival of neurons[9]. It was also demonstrated that the expression of synaptic protein levels was significantly up-regulated and the morphology improved in a transgenic mouse model of Alzheimer's disease treated with NSCs-EVs[30]. On the other hand, intravenous injections of

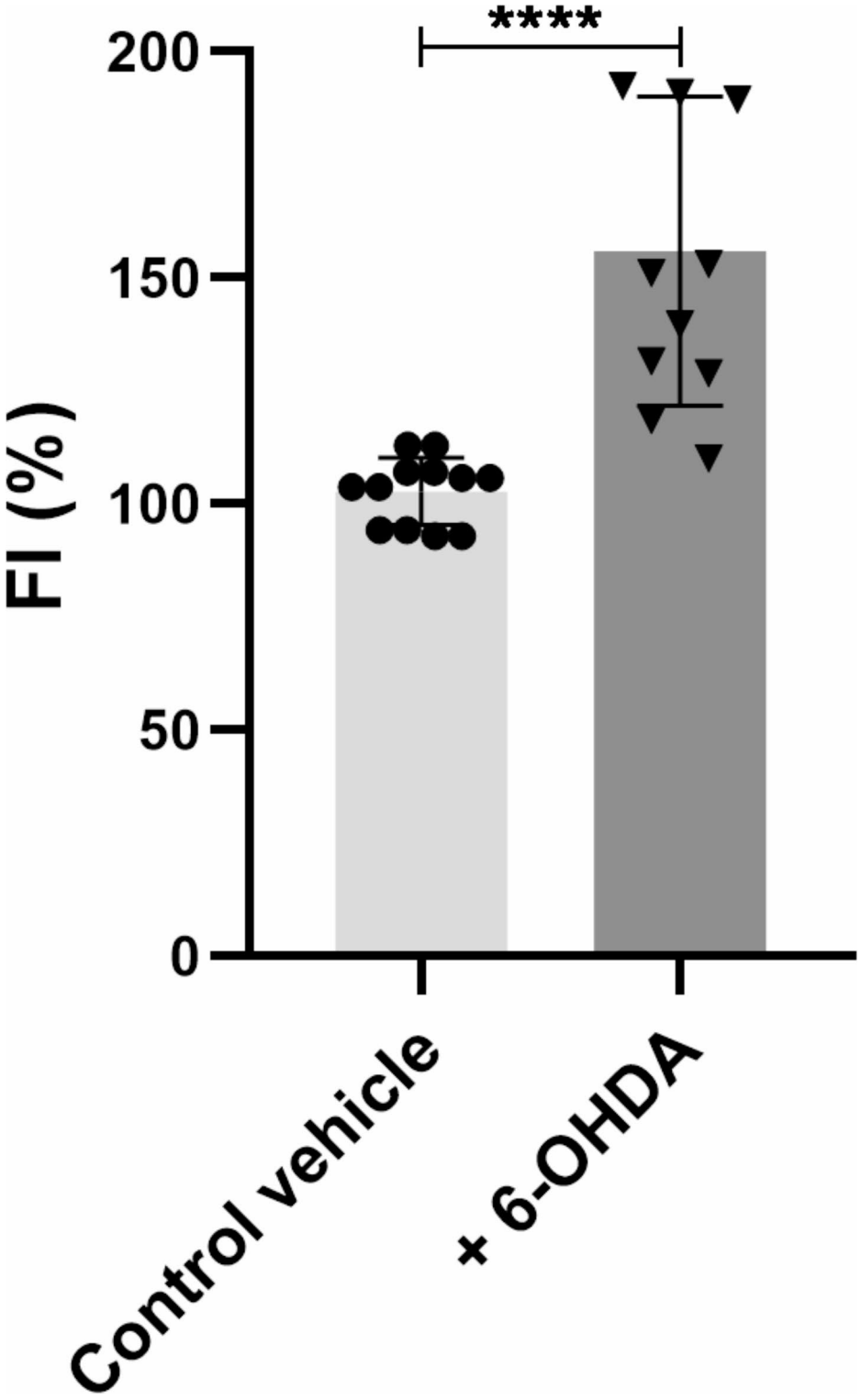

Fig. 8. 6-OHDA increase ROS levels. Effect of 6-OHDA on ROS levels measured by the fluorescence intensity (FI %) of DCFH-DA. Graph represents the mean +/- SD of 3 independent experiments of 10 images each (t-test, **** $p < 0.0001$). 6-OHDA: 6-hydroxydopamine.

human NSC-EVs promote the recovery of motor function in male rats with traumatic brain injury by increasing the migration of endogenous NSCs to the lesion site and the activity of vascular endothelial growth factor (VEGF)[31]. Considering that there is currently no treatment that increases the survival of dopaminergic neurons in Parkinson's patients, we have evaluated the effect of mouse-derived EVs on cell survival in established in vitro PD models. The models showed most of the in vivo features associated with this disease including Synuclein

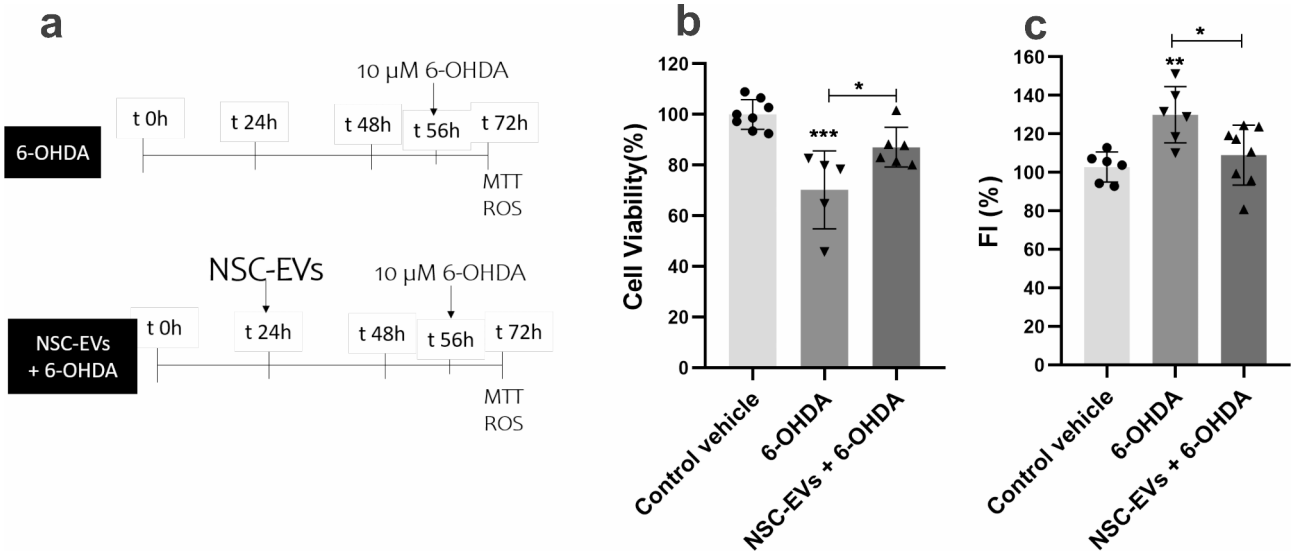

Fig. 9. NSC-EVs protect against the damage generated by 6-OHDA. (**a**) Timeline representation of the experimental protocol. (**b**) Graph represent cell viability (%) obtained by MTT assay. SH-SY5Y cells were preincubated with NSC-EVs and them treated with 10 µM of 6-OHDA. As a control cells were pre-treated with PBS. (**c**) ROS generation in SH-SY5Y cells grown under differentiation conditions, pre-incubated with NSC-EVs and treated with 10 µM of 6-OHDA. Results represent the mean +/- SD of 3 independent experiments each performed in triplicate (One-Way ANOVA; Tukey; * $p < 0.05$; ** $p < 0.01$; *** $p < 0.001$). 6-OHDA: 6-hydroxydopamine, NSC-EVs: extracellular vesicles derived from neural stem cell.

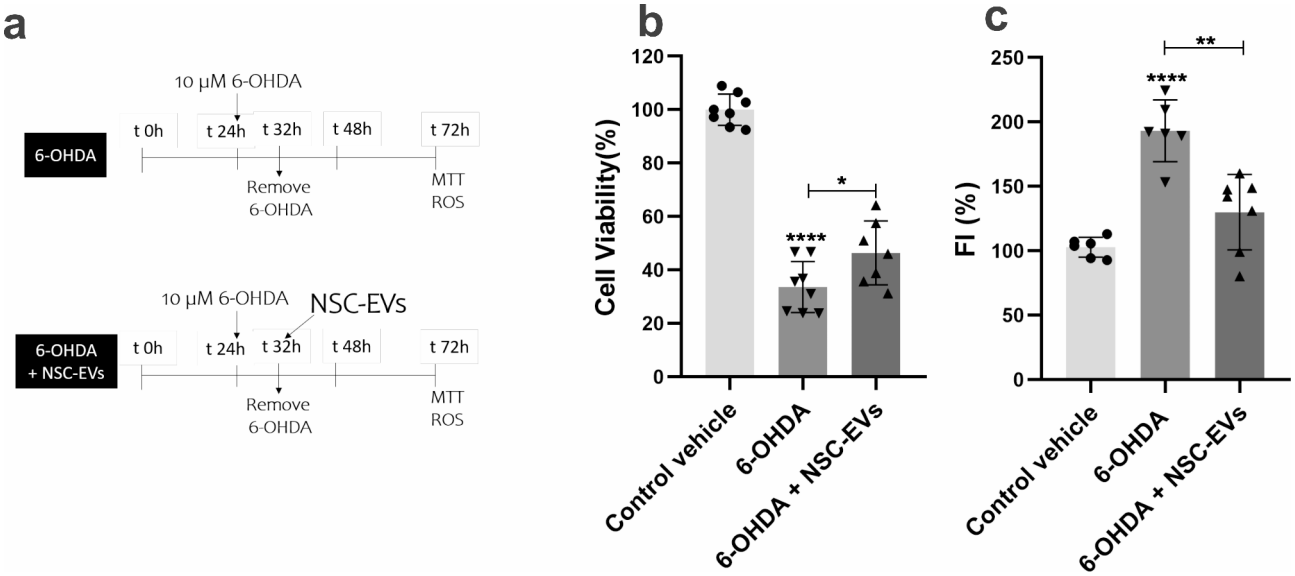

Fig. 10. NSC-EVs reduces the damage generated by 6-OHDA. (**a**) Timeline representation of the experimental protocol. (**b**) Cell viability (%) in cultures of SH-SY5Y cells grown under differentiation conditions, treated with 10 µM of 6OHDA and incubated with NSC-EVs. (**c**) ROS generation in SH-SY5Y cells grown under differentiation conditions, treated with 10 µM of 6OHDA and incubated with NSC-EVs. Results represent the mean +/- SD of 3 independent experiments each performed in triplicate (One-Way ANOVA; Tukey; * $p < 0.05$; ** $p < 0.01$; **** $p < 0.0001$). 6-OHDA: 6-hydroxydopamine, NSC-EVs: extracellular vesicles derived from neural stem cell.

overexpression, mitochondrial dysfunction, cell death by apoptosis and ROS accumulation (Figs. 1 and 8, and Supplementary figures)[3]. In addition, we also demonstrated that 6-OHDA treatment induces the expression of Synuclein at least in the established in vitro model (Fig. 7b).

MTT assay demonstrated that incubation with NSC-EVs increases the survival of cells overexpressing each of the Synuclein variants (Fig. 4). To further analyze if the reduction of metabolically active cells was due to cells

Protein Name	Gene	Uniprot ID	Functions
Vascular cell adhesion molecule 1	Vcam1	Q3UPN1	Tissue repair and regeneration after injury
Glutathione S-transferase kappa 1	Gstk1	A0A0N4SVE5	Oxidoreductase activity. Defense against oxidative and inflammatory stress
Annexin A1	Anxa1	P10107	Innate immune response, anti-inflammatory activity
Thioredoxin	Txn	P10639	Participates in redox homeostasis and oxidative stress response
Catalase	Cat	P24270	Glutathione peroxidase family, involved in defense against oxidative damage
Reticulon-3	Rtn3	Q9ES97	Anti-inflammatory activity by inhibiting NF-kappa-B factor
Peroxiredoxin-2	Prdx2	Q61171	Cellular defense against oxidative stress

Table 2. Proteins involved in oxidative and inflammatory stress defense identified through mass spectrometry analysis of NSC-EVs. The datasets used and analyzed in this study are available from the corresponding author on reasonable request.

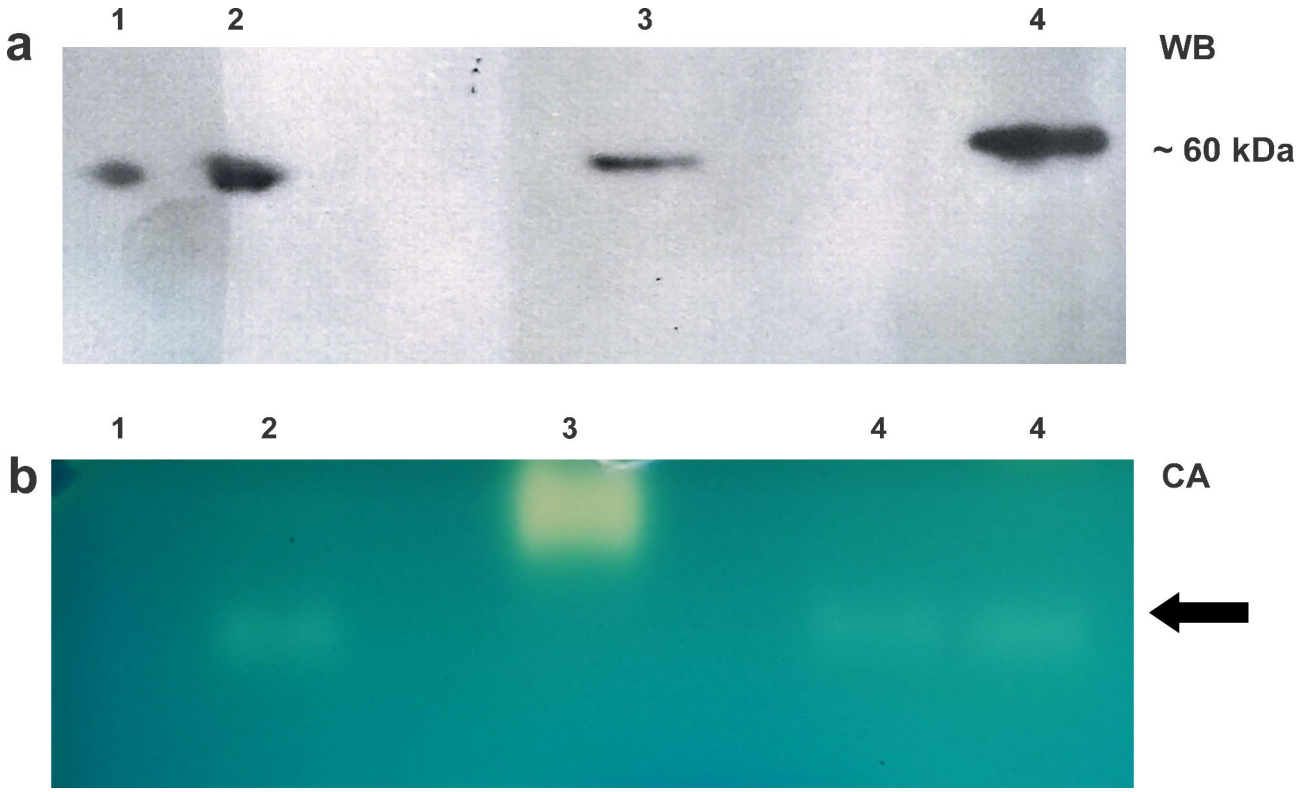

Fig. 11. NSC-EVs are a natural Catalase carrier. (**a**) Representative Western blot (WB) image of Catalase protein level performed using two concentrations of pure catalase as positive controls 0.05 µg (1) and 0.1 µg (2), 15 µg of NSC total protein extract (3) and 15 µg NSC-EVs total protein (4). (**b**) Catalase activity (CA) on native gel from (**1**) BSA (1 µg) as a negative control, pure Catalase (**2**) as a positive control (0.1 µg), 15 µg of NSCs total protein extract (**3**) and 15 µg NSC-EVs total proteins (**4**). The figure displayed here are cropped from the same gels/blot, and without high-contrast (overexposure).

dying, we quantified the percentage of cells that undergo apoptosis or necrosis and demonstrated that NSCs-EVs increase cell viability due to a decrease in apoptosis (Fig. 5).

In the 6-OHDA model, we demonstrated that the presence of EVs before 6-OHDA treatment prevents cell death (Fig. 9); and that the addition of NSC-EVs after 6-OHDA treatment increases cell viability of SH-SY5Y differentiated cells (Fig. 10). These results suggest that NSC-EVs could act in preventing cell death and rescuing the cells affected by 6-OHDA. Similarly, using co-cultured human umbilical MSCs with 6-OHDA-treated SH-SY5Y cells, it was found that cell viability increased, due to a decrease in apoptosis-related proteins and apoptotic rates[15]. Both results confirm that EVs might provide a cytoprotective effect in PD models.

As NSC-EVs increase the survival of dopaminergic neurons which is the main cause of PD, we evaluated the underlying mechanism. We showed that both established models have an increase in oxidative stress (ROS accumulation), a key factor that causes apoptosis in various senile diseases[32–34]. Interestingly and different from previous reports, treatment with NSC-EVs decreases the levels of ROS suggesting an antioxidative effect of these particles.

As mentioned before, the sources of EVs determine the content (proteins, miRNAs, lipids) that drives specific functions[35]. To investigate the protein content of NSC-derived EVs we performed mass-spec proteomic analysis. Interestingly, catalase, a key enzyme that removes H_2O_2[19], was found to be enriched in EVs, suggesting that these small vesicles are a natural "Catalase delivery system". A promising approach for treating Parkinson's disease is reducing reactive oxygen species (ROS) through catalase delivery. However, Catalase's large size prevents it from crossing the BBB. In response, researchers have developed macrophage-derived exosomes loaded with Catalase, demonstrating efficacy in 6-OHDA-induced Parkinson's disease models[36]. Our breakthrough takes this concept further: NSC-derived exosomes, which naturally target neuronal cells and are inherently enriched with catalase, present a vastly superior therapeutic option. This innovation could redefine treatment strategies for neurodegenerative diseases like Parkinson's.

In summary, our study demonstrates the positive effect of NSC-derived EVs on Parkinson's disease models, increasing cell survival and reducing ROS accumulation. Furthermore, we demonstrate that these specific EVs carry activeCatalase enzyme as one of its main cargo. Further studies will allow us to identify other effector molecules carried by the NSC-EVs. Still, the findings of our work shed light on the development of NSC-EVs-based therapeutic strategies to prevent the loss of neurons in neurodegenerative diseases.

Methods

Cell line differentiation

The human neuroblastoma cell line SH-SY5Y (kindly provided by Dr. S. Quiroga U. of Córdoba) was cultured in Dulbecco's modified Eagle's medium (DMEM), 10% fetal bovine serum (FBS) supplemented with penicillin G (100 units/ml), streptomycin (100 µg/ml) (proliferation conditions) and maintained in a 5% CO_2 humidified incubator at 37 °C. For neuronal differentiation conditions, the medium was changed to Dulbecco's modified Eagle's medium (DMEM) supplemented with 2% FBS and retinoic acid (RA) (10 µM) and incubated for at least 48 h. Stable cell lines overexpressing alfa-Synuclein and A53T alfa-Synuclein were established by the transfection with a plasmid (Dr. Benjamin Wolozin (Boston University)) kindly provided the pcDNA3-WT/A53T-α-syn expression vector containing the wild and mutated full length human α-Synuclein sequence) containing the corresponding cDNAs protein sequences followed by a clonal selection in medium containing G418 (cellgro®). Individual clones were screened for overexpression by Western blotting.

Isolation and culture of neural stem cells

Neural stem cells were obtained from fetal mouse brain tissue as previously described[37]. Time pregnant female C57/BL6 mice (gestation day 13) were sacrificed by cervical dislocation under anaesthetic overdose. All the procedures were carried out according to the Guide for the Care and Use of Laboratory Animals (NRC, 2011) and with the approval of the Institutional Ethics and Security Committee (Protocol N° 632/20) of the School of Veterinary Science of the National University of Litoral, Santa Fe, Argentina. The Centre for Comparative Medicine is an entity compliant with GLP for conducting preclinical tests inspected by the Argentine Accreditation Organism (member of the OECD) and the certifications of local regulatory agencies like the ANMAT (National Argentine Administration of Drugs, Food, and Medical Technology,) and the SENASA (National Argentine Service of Animal Sanitation and Food Quality). All procedures were carried out in accordance with the approved guidelines (Guide for the care and use of Laboratory Animals- 8° edition- e National Academies Press-Washington DC 2011 and in compliance with the ARRIVE guidelines).

Briefly the lateral portion of the dorsal telencephalon (cortex) of embryonic day 13 (E13) C57/BL6 mice were isolated and chemically disrupted with trypsin (5 min, 0.05% w/v) and then mechanically disrupted into single cells by repeated pipetting in medium DMEM/F12 (1:1) containing 10% FBS, penicillin G (100 units/ml) and streptomycin (100 µg/mL). After centrifugation (5 min, 1000 rpm) the pellet was resuspended in serum-free medium DMEM/F12 (1:1) and dissociated cells were cultured at a density of 5×10^4 cells/ml in proliferation medium containing DMEM/F12 (1:1) supplemented with B27, 10 ng/ml bFGF and 10 ng/ml EGF and maintained at 37 °C in a humidified 5% CO_2 incubator. After 7 days, primary neurospheres were collected by low-speed centrifugation and dissociated chemically and mechanically into single cells.

Extracellular vesicles isolation and purification

NSC-EVs were purified using size exclusion chromatography qEVoriginal 70 nm (Izon Science, Medford, MA, USA) according to manufacturer's instructions. Briefly, NSCs supernatants were centrifuged at 1,000 g for 10 min and then 10,000 g for 30 min to remove cell debris and passed through a 0.22 µm filter to remove larger vesicles and cellular debris. Cleared conditioned media was concentrated to a final volume of 500 µL using AmiconR Ultra-15 100 kDa filters (Millipore Sigma). EVs separation was performed after column equilibration at room temperature. Fractions of 0.5 mL were collected using PBS as eluent. Four EVs-rich fractions (7–10) were pooled and either analysed directly or concentrated using an AmiconR Ultra-4 100 kDa centrifugal filters.

Characterization of extracellular vesicles

Particles size and their distributions were calculated and measured by a nanoparticle tracking analysis (NTA) with ZetaView PMX-230 Twin Laser (Particle Metrix) according to guidelines of MISEV2023[38]. For real-time visualization of Brownian Motion and electrophoretic mobility the measuring size is 10–1000 nm and concentration range are 10^5–10^9 particles/mLn. For Zeta potential, the working range is − 500 mV to + 500 mV, concentration range is 10^6–10^{10} particles/mL and conductivity range are 3 µS/cm–15 mS/cm.

Negative staining of EVs suspensions followed by imaging in a transmission electron microscope (TEM) was used to determine vesicle shape and size distribution. Briefly, 10 µl aliquots of EVs suspension were dispensed onto sheets of Parafilm in a humidified petri dish and the vesicles were deposited on carbon-coated grid (300–400 mesh) for 3–5 min. Afterwards, the sample was negatively stained with 2% uranyl acetate for 3–5 min.

The excess stain was removed with filter paper and the grid was briefly washed with Mili-Q water and air-dried for 15 min at RT. Images were taken using a JEOL-JEM2100plus, at the Facility for Transmission Electron Microscopy of the IFIR (CONICET).

EVs-Protein markers Tetraspanin, Alix (1/500) and TSG 101 (1/500) were determined by immunoblotting and by proteomic analysis (Table 1). In addition, dynamic light scattering (DLS) was performed to determinate EVs size.

Labelling of EVs

For labelling, 37 µl (1×10^8 particles) of EVs in PBS were mixed with 1 µg/mL of FM® 4–64 (Molecular ProbesTM) and incubated for 1 h at 4°C. Next, NSC-EVs were added to SH-SY5Y, and the uptake of EVs was immediately monitored by in vivo confocal microscopy (Zeiss LSM 880) and qualitative analyses were performed with Image J" (NIH). As a negative control, cells were treated with the same dilution of FM® 4–64 in PBS.

Western blot

For western blot analysis, cells were plated at a density of 5×10^5 /100-mm dish for 24 h, after which the medium was changed to DMEM supplemented with 2% FBS and RA (10 µM). After 48 h, cells were collected and resuspended in 1X RIPA buffer (25 mM Tris.HCl pH 7.6, 150 mM NaCl, 1% NP-40, 1% sodium deoxycholate, 0.1% SDS was used and 1:1000 cocktail (Sigma)). Proteins concentrations were determined using Bovine Serum Albumine (BSA) as standard protein and "Pierce BCA Protein Assay Kit" (Thermo Scientific). 15 µg of cell lysate was resolved on 12% SDS-polyacrilamide gel electrophoresis (PAGE) and transferred to a nitrocellulose membrane (Amersham, GE Healthcare). After blocking overnight (ON) with 5% non-fat milk in 0.1% Tween TBS and washing, blots were incubated ON with anti-TSG-101 (1:500; Santa Cruz), anti-ALIX (1/1000; abcam), anti-α-Synuclein (1/1000; BD) or anti-catalase (1/1000, abcam). As secondary antibody peroxidise-conjugated anti-rabbit/anti-mouse (1/10000; Jackosn Immuno Research) was used. For loading protein control anti-GAPDH (1/1000; Santa Cruz), anti-β-Actin (1/1000; Santa Cruz), anti-Calnexin (1/1000, abcam) and anti-Prohibitin (1/500; Santa Cruz) was used and developed with secondary antibody peroxidase-conjugated anti-mouse/anti-rabbit IgG (1:8000, Jackson Immuno Research). Labelled proteins were detected with chemiluminescence reagents (AmershamTM ECLTM Prime Western Blotting Detection Reagent, GE Healthcare).

Immunocytochemistry

6×10^4 cells were cultured on glass coverslips in 24-well plates. After the desired incubation period, cells were fixed in 4% (w/v) paraformaldehyde-sucrose for 30 min at room temperature, permeabilized with 0.2% Triton X100 and blocked for 1 h in 5% BSA. Cells were incubated with the primary antibody overnight at 4°C followed by incubation with the fluorescently labelled secondary antibody for 1 h at room temperature. Primary and secondary antibodies were diluted as follows: rabbit anti-α-Synuclein (1:700; BD), mouse anti-β-III tubulin (1:500; Merck), anti-rabbit Alexa Fluor® 488-labelled (1:300; Thermo Fisher) and anti-mouse Cy3-labelled (1:500). To visualize nuclei, cells were counterstained with Hoechts. Micrographs were acquired using a confocal microscope (Zeiss LSM 880) and quantitative analyses were performed with Image J (NIH).

Viability assay

Cell viability was assessed by MTT-reduction assay[13]. After cell treatment, MTT (5 mg/ml) was added to the cell culture medium at a final concentration of 0.5 mg/ml and incubated for 4 h at 37 °C, 5% CO_2. The assay was stopped by replacing the MTT-containing medium with DMSO. The extent of MTT reduction was measured spectrophotometrically at 570 nm in Synergy 2 Multi-Mode Microplate Reader (BioTek). Results are expressed as a percentage of the control.

Cell death assay

The double staining assay with the fluorescent probes Ethidium Bromide (EB), and Acridine Orange (AN), allows characterization of the type of cell death by apoptosis or necrosis[14]. After two washes with PBS, EB (0.1 mg/ml) and AN (0.1 mg/ml) were added and incubated 5 min at room temperature. Then, two more washes were performed with PBS and nuclear morphology was immediately observed on Olympus IMT2 inverted fluorescence microscope. Images were taken and analyzed using Image J" software (NIH). We distinguished four types of cells according to the fluorescence emission and the morphological aspect of chromatin condensation in the stained nuclei. (1) Viable cells have uniform bright green nuclei with organized structure (PMNCs also have orange cytoplasm). (2) Early apoptotic cells (which still have intact membranes but have started to undergo DNA cleavage) have green nuclei, but perinuclear chromatin condensation is visible as bright green patches or fragments. (3) Late apoptotic cells have orange to red nuclei with condensed or fragmented chromatin. (4) Necrotic cells have a uniformly orange to red nuclei with organized structure.

Quantitative evaluation of intracellular ROS levels

To evidence the presence of intracellular reactive oxygen species (ROS), the fluorescent probe 2′,7′-dichlorodihydrofluorescein diacetate (DCFH-DA) was used[39]. After three washes with PBS, cells were incubated with 10 µM DCFH-DA probe in the dark for 30 min. After this time, cells were washed with PBS three times and fluorescence was observed used the Synergy 2 Multi-Mode Microplate Reader (λexc: 488 nm, λem: 520 nm; BioTek). Finally, three washes were performed with PBS to remove excess probe and cells were lysed with 50 µL of hypotonic lysis buffer (Tris pH 8 50 mM, KCl 50 mM, EDTA 10 mM, Nonidet P-40 1%) on ice. Subsequently, protein concentration of each lysate was determined using Bovine Serum Albumine (BSA) as standard protein and "Pierce BCA Protein Assay Kit" (Thermo Scientific). The fluorescence intensity (FI) per µg of protein was relativized for each condition. Results are expressed as a percentage (FI%) of the control.

Catalase-peroxidase activity gel

Catalase-peroxidase activity gels were based on a previously reported assay[20–22]. Briefly, NSC were pelleted, and frozen at −80 °C. Cells were resuspend in lysis buffer (50 mM Tris-HCl pH 8.0, 50 mM KCl, 10 mM EDTA, 20 mM NaF, 1 mM Na_3VO_4, 1mM PMSF, 50 mM TPCK and 1:1000 cocktail (Sigma)). Proteins concentrations were determined using Bovine Serum Albumine (BSA) as standard protein and "Pierce BCA Protein Assay Kit" (Thermo Scientific). 15 µg of NSC-EVs, NSC- extract (15 µg) and pure Catalase as a control (0.1 µg) was resolved on 8% native-PAGE at 4 °C for 4 h. The catalase gel was washed in ultrapure water three times for 15 min each and then incubated with 30% $H_2O_2$for 10 min. The gel was rinsed and added to a mixture of equivalent volumes (25 mL total) of 2% potassium ferricyanide and 2% iron chloride to stain the gel. Hydrogen peroxide reduces potassium ferricyanide (III) to potassium ferrocyanide (II); the peroxide is oxidized to molecular oxygen. Ferric chloride reacts with ferrocyanide (II) to form stable, insoluble Prussian Blue pigment[21,20–22,40]. The gel was rocked by hand until a faint green color started to appear in the gel, and then the gel was transferred to water and imaged. Catalase bands appeared clear or yellow on the green background of the gel. Gel images were converted to grayscale for easier viewing in print.

LC-MS analysis

For proteomics, three samples of NSC-EVs purified using Izon columns were collected and lysed in 1X PBS with 1% sodium dodecyl sulphate (SDS) and protease inhibitors cocktail 1X (Sigma). Protein extraction was performed by 5 cycles of 30 s of sonication[41].Samples were then centrifuged at 14,000 g for 10 min at 4 °C, and supernatant containing protein was keep for subsequent analysis protein concentration was measured with BCA Protein Assay (Thermo Fisher Scientific) using BSA as a standard. For protein digestion, approximately 5 µg of proteins were loaded in 12% polyacrylamide gel and tryptic digestion of the corresponding fragments was carry following the protocol described by Link y LaBaer (2009)[18].

Mass spectrometric analysis was performed at the Mass Spectrometry Unit of the Institute of Molecular and Cellular Biology of Rosario (UEM-IBR), Argentina. Peptide separations were carried out on a nanoHPLC Ultimate3000 (Thermo Scientific) using a nano column EASY-Spray ES901 (15 cm × 50 µm ID, PepMap RSLC C18). The mobile phase flow rate was 300 nL/min using 0.1% formic acid in water (solvent A) and 0.1% formic acid and 100% acetonitrile (solvent B). The gradient profile was set as follows: 4–30% solvent B for 64 min, 30–80% solvent B for 7 min and 80% solvent B for 2 min. Three microliters of each sample were injected. MS analysis was performed using a Q-Exactive HF mass spectrometer (Thermo Scientific). For ionization, 1,9 kV of liquid junction voltage and 250 °C capillary temperature was used. The full scan method employed a m/z 375–1600 mass selection, an Orbitrap resolution of 120,000 (at m/z 200), a target automatic gain control (AGC) value of 3e6, and maximum injection times of 100 ms. After the survey scan, the 20 most intense precursor ions were selected for MS/MS fragmentation. Fragmentation was performed with a normalized collision energy of 27 eV and MS/MS scans were acquired with a dynamic first mass, AGC target was 5e5, resolution of 30,000 (at m/z 200), intensity threshold of 4.0e4, isolation window of 1.4 m/z units and maximum IT was 200 ms. Charge state screening was enabled to reject unassigned, singly charged, and equal or more than seven protonated ions. A dynamic exclusion time of 15 s was used to discriminate against previously selected ions.

Protein identification and data analysis

Raw data from the Orbitrap Q-Exactive were analyzed using Maxquant software package (v2.1.4.0) using standardized workflows[42,43]. For label-free peptide quantitation by MS1-intensity and peptides (proteins) were identified using the built-in Andromeda search engine. Mass spectra files were searched against the database of Mus musculus (Mouse) from Uniprot (UP000000589- date: 18/04/23). All searches were performed with tryptic specificity allowing two missed cleavages. The database searches were performed with carbamidomethyl I as fixed modification and acetylation (protein N terminus) and oxidation (M) as variable modifications. Mass spectra were searched using the default setting of MaxQuant namely a false discovery rate of 1% on the peptide and protein level. The data generated using MaxQuant was uploaded into Perseus software v1.6.13.0 to identify EVs containing proteins and filtered from contaminants.

Statistical analysis

Data represent the mean value ± SD of at least three independent experiments and each individual experiment was performed in technical triplicate. Statistical significance was determined, as appropriate, by either Student's t-test or One-Way ANOVA followed by Dunnett or Tukey's test using Prism (GraphPad Software Inc.,). p-values lower than 0.05 were considered statistically significant.

Data availability

The datasets used and analyzed in this study are available from the corresponding author on reasonable request.

Received: 2 September 2024; Accepted: 17 January 2025
Published online: 19 February 2025

References

1. Dorsey, E. R. et al. Global, regional, and national burden of Parkinson's disease, 1990–2016: A systematic analysis for the global burden of Disease Study 2016. *Lancet Neurol.* **17**, 939–953 (2018).
2. Sveinbjornsdottir, S. The clinical symptoms of Parkinson's disease. *J. Neurochem.* **139** (Suppl 1), 318–324 (2016).
3. Schlachetzki, J. C., Saliba, S. W. & Oliveira, A. C. Studying neurodegenerative diseases in culture models. *Braz. J. Psychiatry* **35** (Suppl 2), S92–100 (2013).
4. Connolly, B. S. & Lang, A. E. Pharmacological treatment of Parkinson disease: A review. *JAMA* **311**, 1670–1683 (2014).

5. Pardo-Moreno, T. et al. Current treatments and new, tentative therapies for Parkinson's disease. *Pharmaceutics* **15**, 770 (2023).
6. Witwer, K. W. & Wolfram, J. Extracellular vesicles versus synthetic nanoparticles for drug delivery. *Nat. Rev. Mater.* **6**, 103–106 (2021).
7. van Niel, G., D'Angelo, G. & Raposo, G. Shedding light on the cell biology of extracellular vesicles. *Nat. Rev. Mol. Cell. Biol.* **19**, 213–228 (2018).
8. Wiklander, O. P. B., Brennan, M. A., Lotvall, J., Breakefield, X. O. & El Andaloussi, S. Advances in therapeutic applications of extracellular vesicles. *Sci. Transl. Med.* **11**, eaav8521 (2019).
9. Ocaña, S. D., Magaquian, D. & Banchio, C. J. F.i.M.N. neural stem cell-derived extracellular vesicles favour neuronal differentiation and plasticity under stress conditions. *Front. Mol. Neurosci.* **16**, 1146592 (2023).
10. Kirik, D. et al. Parkinson-like neurodegeneration induced by targeted overexpression of α-synuclein in the nigrostriatal system. *J. Neurosci.* **22**, 2780–2791 (2002).
11. Lázaro, D. F. et al. Systematic comparison of the effects of alpha-synuclein mutations on its oligomerization and aggregation. *PLoS Genet.* **10**, e1004741 (2014).
12. Raza, C., Anjum, R. & Shakeel N.U.A. Parkinson's disease: Mechanisms, translational models and management strategies. *Life Sci.* **226**, 77–90 (2019).
13. Mosmann, T. Rapid colorimetric assay for cellular growth and survival: Application to proliferation and cytotoxicity assays. *J. Immunol. Methods*. **65**, 55–63 (1983).
14. Baskić, D., Popović, S., Ristić, P. & Arsenijević N. N. Analysis of cycloheximide-induced apoptosis in human leukocytes: Fluorescence microscopy using annexin V/propidium iodide versus acridin orange/ethidium bromide. *Cell. Biol. Int.* **30**, 924–932 (2006).
15. Chen, H. X. et al. Exosomes derived from mesenchymal stem cells repair a Parkinson's disease model by inducing autophagy. *Cell Death Dis.* **11**, 288 (2020).
16. Ebadi, M., Srinivasan, S. K. & Baxi, M. D. Oxidative stress and antioxidant therapy in Parkinson's disease. *Prog. Neurobiol.* **48**, 1–19 (1996).
17. de Almeida, A. et al. ROS: Basic concepts, sources, cellular signaling, and its implications in aging pathways. *Oxid. Med. Cell. Longev.* **2022**, 1225578 (2022).
18. Link, A. J. & Labaer, J. In-gel trypsin digest of gel-fractionated proteins. *Cold Spring Harb Protoc*, pdb prot5110 (2009).
19. Aebi, H. & Catalase. In *Methods of Enzymatic Analysis* 673–684 (Elsevier, 1974).
20. Scandalios, J. G. Genetic control of multiple molecular forms of catalase in maize. *Ann. N. Y. Acad. Sci.* **151**, 274–293 (1968).
21. Woodbury, W., Spencer, A. K. & Stahman, M. A. An improved procedure using ferricyanide for detecting catalase isozymes. *Anal. Biochem.* **44**, 301–305 (1971).
22. Wayne, L. G. & Diaz, G. A. A double staining method for differentiating between two classes of mycobacterial catalase in polyacrylamide electrophoresis gels. *Anal. Biochem.* **157**, 89–92 (1986).
23. Kourembanas, S. Exosomes: Vehicles of intercellular signaling, biomarkers, and vectors of cell therapy. **77**, 13–27 (2015).
24. Palanisamy, C. P. et al. New strategies of neurodegenerative disease treatment with extracellular vesicles (EVs) derived from mesenchymal stem cells (MSCs). *Theranostics* **13**, 4138–4165 (2023).
25. Zhang, L. et al. Exogenous plant MIR168a specifically targets mammalian LDLRAP1: Evidence of cross-kingdom regulation by microRNA. *Cell. Res.* **22**, 107–126 (2012).
26. Cao, M. et al. Ginseng-derived nanoparticles alter macrophage polarization to inhibit melanoma growth. *J. Immunother Cancer*. **7**, 326 (2019).
27. De Robertis, M. et al. Blueberry-derived exosome-like nanoparticles counter the response to TNF-α-induced change on gene expression in EA. hy926 cells. *Biomolecules* **10**, 742 (2020).
28. Hong, S. W. et al. Extracellular vesicles derived from Staphylococcus aureus induce atopic dermatitis-like skin inflammation. *Allergy* **66**, 351–359 (2011).
29. Kim, M. R. et al. S taphylococcus aureus-derived extracellular vesicles induce neutrophilic pulmonary inflammation via both T h1 and T h17 cell responses. *Allergy* **67**, 1271–1281 (2012).
30. Li, B. et al. Impact of neural stem cell-derived extracellular vesicles on mitochondrial dysfunction, sirtuin 1 level, and synaptic deficits in Alzheimer's disease. *J. Neurochem.* **154**, 502–518 (2020).
31. Sun, M. K. et al. Extracellular vesicles mediate neuroprotection and functional recovery after traumatic brain injury. *J. Neurotrauma* **37**, 1358–1369 (2020).
32. Harman, D. Alzheimer's disease pathogenesis: Role of aging. *Ann. N. Y. Acad. Sci.* **1067**, 454–460 (2006).
33. Saxena, S., Mathur, A. & Kakkar, P. Critical role of mitochondrial dysfunction and impaired mitophagy in diabetic nephropathy. *J. Cell. Physiol.* **234**, 19223–19236 (2019).
34. Lin, H. J., Wang, X., Shaffer, K. M., Sasaki, C. Y. & Ma, W. Characterization of H2O2-induced acute apoptosis in cultured neural stem/progenitor cells. *FEBS Lett.* **570**, 102–106 (2004).
35. Zaborowski, M. P., Balaj, L., Breakefield, X. O. & Lai, C. P. Extracellular vesicles: Composition, Biological relevance, and methods of study. *Bioscience* **65**, 783–797 (2015).
36. Haney, M. J. et al. Exosomes as drug delivery vehicles for Parkinson's disease therapy. *J. Controlled Release*. **207**, 18–30 (2015).
37. Costa, M. R., Wen, G., Lepier, A., Schroeder, T. & Götz, M. Par-complex proteins promote proliferative progenitor divisions in the developing mouse cerebral cortex. *Development* **135** (2008).
38. Welsh, J. A. et al. Minimal information for studies of extracellular vesicles (MISEV2023): From basic to advanced approaches. *J. Extracell. Vesicles.* **13**, e12404 (2024).
39. LeBel, C. P., Ischiropoulos, H. & Bondy, S. C. Evaluation of the probe 2', 7'-dichlorofluorescin as an indicator of reactive oxygen species formation and oxidative stress. *Chem. Res. Toxicol.* **5**, 227–231 (1992).
40. Donegan, R. K. et al. Exogenously scavenged and endogenously synthesized Heme are differentially utilized by Mycobacterium tuberculosis. *Microbiol. Spectr.* **10**, e0360422 (2022).
41. Bonafede, R. et al. The anti-apoptotic effect of ASC-exosomes in an in vitro ALS model and their proteomic analysis. *Cells* **8**, 1087 (2019).
42. Cox, J. & Mann, M. MaxQuant enables high peptide identification rates, individualized ppb-range mass accuracies and proteome-wide protein quantification. *Nat. Biotechnol.* **26**, 1367–1372 (2008).
43. Tyanova, S., Temu, T. & Cox J. The MaxQuant computational platform for mass spectrometry-based shotgun proteomics. *Nat. Protocols* **11**, 2301–2319 (2016).

Acknowledgements

This work was supported by Consejo Nacional de Investigaciones Científicas y Técnicas (CONICET), Agencia Nacional de Promoción Científica y Tecnológica (ANPCyT) PICT 2019-01073). Authors thank to Dr. Benjamin Wolozin for kindly providing the WT/A53T α-syn DNA construct, to Drs. Hugo Gramajo and Consuelo Perez for critical reading of the manuscript, to Dr. E. Morales and Tec. R. Vena for excellent support in confocal microscopy analysis, to D. Campos for technical assistant, to Drs. Eduardo Ceccarelli, Germán Rosano and Lic. Alejo Cantoia for the support in proteomic analysis.

Author contributions

Author Contributions M.D.R performed all the experiments and analyzed data and prepare Figures; S.G carried out standardization of the in vitro models and prepare Supplemented Figures, S.D. analyzed the proteomic data and prepared Table 1; H.H.O. carried out animal procedures; C.B. designed and supervised research, acquired funding and wrote the manuscript.

Declarations

Competing interests

The authors declare no competing interests.

Additional information

Supplementary Information The online version contains supplementary material available at https://doi.org/10.1038/s41598-025-87238-7.

Correspondence and requests for materials should be addressed to C.B.

Reprints and permissions information is available at www.nature.com/reprints.

Publisher's note Springer Nature remains neutral with regard to jurisdictional claims in published maps and institutional affiliations.